J. Ind. Geophys. Union, 28(6) (2024), 404-416

Sources of errors and basic corrections to Swarm satellite magnetic data for lithospheric magnetic anomaly modelling

Monica Rawat[1*], S.P. Anand[1], Shaik Kareemunnisa Begum[2]
[1] Indian Institute of Geomagnetism, New Panvel, Navi Mumbai- 410218, India.
[2]Department of Geophysics, Andhra University, Visakhapatnam- 530003, India.
*Corresponding author: monicarawat10@gmail.com

ABSTRACT

Accurate measurements of Earth's magnetic field from low-earth orbit satellites, such as those conducted by the Swarm mission, capture the complex overlapping of various internal and external magnetic sources that coexist in both time and space. Among these sources, the Earth's lithospheric field is notably one of the weakest detectable signals from space. Achieving a precise description of this field. necessitates meticulous handling of rapidly fluctuating magnetic fields originating from the ionosphere and magnetosphere, along with core fields and other potential sources of error. Before employing magnetic data for inversion processes for lithospheric field modelling, it is crucial to ensure that the input data is devoid of noise. Clean datasets significantly enhance the accuracy of lithospheric models, thereby revealing more detailed geological features and providing richer geophysical information about the study areas. This paper outlines some of the basic sources and the corrections applied to the magnetic field measured by satellites, to enhance the magnetic field of the lithosphere from the background magnetic fields associated with the main and external magnetic sources. These include environmental selection criteria, background field removal, temporal corrections like trend removal, filtering etc. The importance of manual correction and treatment of these fields is also emphasized, as these steps are crucial for revealing the subtle features of the lithospheric magnetic field.

Keywords:

Swarm constellation, Lithospheric models, Kp and Dst index, Earth’s magnetic field, Magnetic anomaly modelling,

INTRODUCTION

The magnetic field of the Earth can be measured from different platforms like ground, aircraft, helicopters, ships, and satellites, each with different resolution and wavelength information (Mandea and Purucker, 2005). Compared to the magnetic field measurements from other platforms, measurements onboard satellites have the advantage of sampling the magnetic field over the entire Earth with the same instrumentation, which can provide well-distributed set of observations in generating magnetic field models. Different satellites have been launched in the past 50 years with a motive to study the earth’s magnetic environment. The magnetic field observed from different platforms is the superposition of magnetic field originating from three different sources: the main (or internal) field originating from sources in the Earth’s outer core (dynamo effect), the crustal field arising from the magnetized rocks in the crust and upper most mantle and external field, whose sources lies in the ionosphere-magnetosphere, which is highly dependent on the solar activity. Besides these, there is an oceanic magnetic field also, generated due to ocean circulation, which is the weakest. These aforementioned fields range in amplitude from a few nanoteslas to thousands of nanotesla and overlap one another in space and time (Olsen and Stole, 2012; Finlay et al., 2016) in such a way that the isolation of individual fields remains one of the major issues in geomagnetic field modelling. In 1838, using spherical harmonic expansion of the geomagnetic field, C.F. Gauss developed a method to roughly separate the internal and external contributions to the field. Since then, several mathematical models have been developed to represent the magnetic field generated by internal and external sources (Shure et al., 1982; Haines, 1985; Langel, 1990; Hulot et al., 2015). The satellite missions with magnetometer onboard proved to be very advantageous in modeling the varied fields such as lithospheric, core, ionospheric and magnetospheric fields and to explain the phenomenon behind the various sources of the magnetic field of the Earth (Stolle et al., 2016).

The isolation of Earth's lithospheric magnetic field from other overlapping magnetic fields presents a fundamental challenge in lithospheric field modeling (Thebault et al., 2010). The development of local lithospheric models crucially depended on a sequence of spacecraft launches, which aid in understanding not only the lithosphere, but also broader fields like the Earth's core and magnetosphere. The lithospheric field is one of the weakest field (around 0.01% of the measured field) captured by magnetometers onboard satellites at altitudes of over 400 km (Thebault et al., 2017). Since this field is masked by the strong background fields arising from core and external sources, careful treatment is required to unveil this weak signal from a strong background. Approaches followed to model the lithospheric fields from the satellite observations can be grouped into comprehensive and serial, each having advantages and limitations (Hulot et al., 2015). The comprehensive modeling approach utilizes the available observatory and satellite data to co-estimate models of both internal and external origin, through an extensive inversion process (Hulot et al., 2015). Recently generated lithospheric models through a comprehensive approach, include CM6 (Sabaka et al., 2020), CHAOS (Finlay et al., 2020), and LCS-1 (Olsen et al., 2017). The sequential or serial approach involves step-by-step processing of the observed data to remove the field sources other than the lithospheric field and apply empirical correction to it (Maus et al., 2007). The Magnetic Field (MF) model series are example of this type of approach. Enhanced processing methods were implemented in MF7 (Maus et al., 2010) to analyze lithospheric field data effectively.

Of late several regional lithospheric models have been developed from satellite magnetic field measurements, employing varied processing and modelling techniques. Regional lithospheric models have an advantage over global models, as the latter provide information on long wavelength anomalies. Regional lithospheric models have been generated over India (Singh and Rajaram, 1990), China and adjoining regions (Zhang et al., 2018), Egypt (Fathy and Ghamry, 2021; Abdellatif et al., 2022), Balkan (Abramova et al., 2014), Siberia (Abramova and Abramova, 2014), Africa (Vervelidou et al., 2018), Tibet (Qiu et al., 2017) etc utilizing data from different satellite missions. Rawat et al. (2024) derived a lithospheric magnetic anomaly model over the Indian region (LAMI-1) from 7 years of magnetic data acquired by Swarm satellites A and C, using damped least square inversion. The magnetic field emanating from Earth's lithosphere, primarily results from lateral variations in the magnetization of rocks in the lithosphere (Purucker and Clark, 2011**)**. This field carries valuable information about the composition and magnetization of subsurface rock formations, providing insights into geological block ages, depths, and overall crustal structure **(**Purucker et al., 2002**).** Furthermore, it can indirectly shed light on the thermal regime and tectonic evolution of Earth's crust. Accurately deciphering the geographical nuances of the lithospheric magnetic field is not only critical for navigation purposes but also demands consistent, high-quality data spanning vast distances, from continental boundaries to satellite altitudes. The development of lithospheric models heavily relies on satellite measurements and the processing of the observed data to isolate the weak lithospheric signals. The limitations of individual satellite missions in terms of data coverage over space and time have led to challenges in accurately separating and characterizing contributions from different sources (Agarwal et al., 1986) that has been overcome in the recent years due to increased satellite missions.

As discussed earlier, the amplitude of the lithospheric field is minuscule at satellite altitude. A proper selection criteria such as selecting days with low geomagnetic activity, processing methodology including removal of incomplete passes, removal of main field and external field etc., have to be followed to isolate the lithospheric signature from the strong background signal. The objective of this paper is to elucidate the various processes employed to eliminate unwanted field signals and to isolate the lithospheric field with examples from satellite data, acquired over the Indian region and its adjacent oceanic areas. It digs into the methodologies and corrections that can be applied to effectively reduce these extraneous signals, thereby enhancing the accuracy of the lithospheric field extraction. In addition, it is believed that the meticulous correction depicts the lithospheric features hidden behind the erroneous field.

DATA SELECTION AND CORRECTION

The deployment of the Swarm constellation by the European Space Agency (ESA) in November 2013, represents a significant advancement in providing high-quality data for different sources of external and internal fields (Olsen et al., 2015). This mission is designed to gather magnetic field measurements along three distinct orbital paths that substantially enhance the spatial and temporal resolution of Earth's dynamic and static magnetic fields. The Swarm mission's Level 1b data products include time-series measurements that have been quality-screened, calibrated, and corrected, all presented in physical SI units and geo-referenced coordinates (https://swarmhandbook. earth.esa.int). These data sets are generated daily and are separately provided for each of the three satellites: Swarm A, Swarm B, and Swarm C. Swarm satellite low resolution (1Hz) data has been subjected to correction for a better improvement of lithospheric model and these corrections have been described in a comprehensive way later. The Swarm satellite is equipped with a fluxgate magnetometer (FGM) that captures three orthogonal vector components: North, East, and Center. These vector measurements are utilized for extracting the lithospheric magnetic anomaly field. To achieve this, the data undergoes a series of sophisticated processing stages designed to refine and enhance the accuracy of the magnetic anomaly models. The process of assembling corrected data, with very limited noise, for constructing the lithospheric field revolves around three distinct categories: environmental selection, background removal, and temporal selection. Better understanding and correction of these categories ensure the accuracy of the resulting model. Processing steps and correction applied to data observed onboard satellites, for improvement of lithospheric model, is similar to Swarm satellite constellation (Sat A, B and C) low resolution (1Hz) data. In this paper we discuss the processing steps with reference to Satellite A and C, as they are at a lower orbital altitude than satellite B, hence will have improved wavelength resolution. However, data from satellite B (after corrections) in conjunction with A and C, can be is used to compute the vertical gradient of the lithospheric magnetic field.

Environmental selection

Environmental selection entails the careful curation of data based on environmental factors, such as effects from ring currents and solar wind creating geomagnetic storms. This involves identifying and excluding data points that may be influenced by external factors or disturbances. Within the realm of space weather research, the focus lies on understanding the dynamics of the geomagnetic field during satellite measurements. Space weather conditions delineate variations in geomagnetic behavior under the influence of external currents, quantified through indices (Kp and Dst) during both quiet and perturbed conditions. The Kp-index (Matzka et al., 2021), serves as a local measure of geomagnetic disturbances, ranging in scale from 0 to 9. It is derived from 13 selected observatories, distributed in sub-auroral latitudes and quantifies fluctuations in the horizontal component of Earth's magnetic field over three-hour intervals. The Kp index ranges from 0 to 9, indicating levels of geomagnetic activity. A value of 1 denotes quiet conditions, while 3 or higher signifies a geomagnetic storm. Kp index variations from 2014 to 2020 are shown in **Figure1**.

For effective model computation, days with a Kp index between 0 and 2 are particularly useful. The data shows there are enough days with such a low Kp index within this period (2014 to 2020) to ensure accurate model calculations. The magnetic field fluctuations (Z component) recorded at two magnetic observatories viz., Alibag and Gulmarg during geomagnetically quiet (Kp=1) (Figure 2a) and disturbed conditions (Kp =3) (Figure 2b) is demonstrated in Figures 2a,b. In both scenarios, it can be seen that the daytime geomagnetic field exhibit significant fluctuations, whereas, the night-time values remained relatively less fluctuating. Upon comparing the night-time field data between the two conditions (Kp =1 and 3^+), it can be seen that during quiet periods, the night-time field values were less variable, indicating low geomagnetic activity, whereas data of night time field values during disturbed days were relatively variable and hence the data acquired during this period is not considered. This makes such conditions ideal for regional lithospheric modeling, where it is preferable to select data from the days when night-time field values are least noisy, ensuring more accurate results.

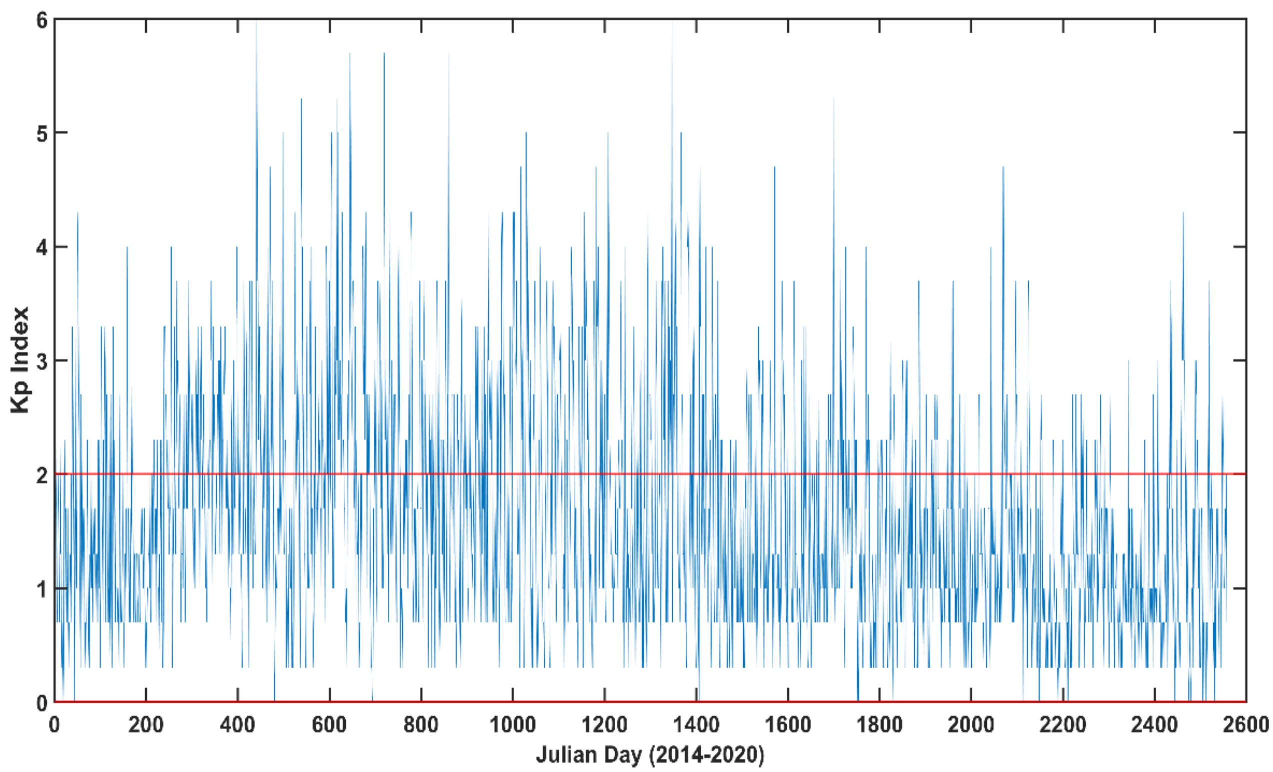

Figure 1. Yearly Kp index data, depicted in Julian day format for the years 2014 to 2020. The red line represent the selection of kp less than 2.

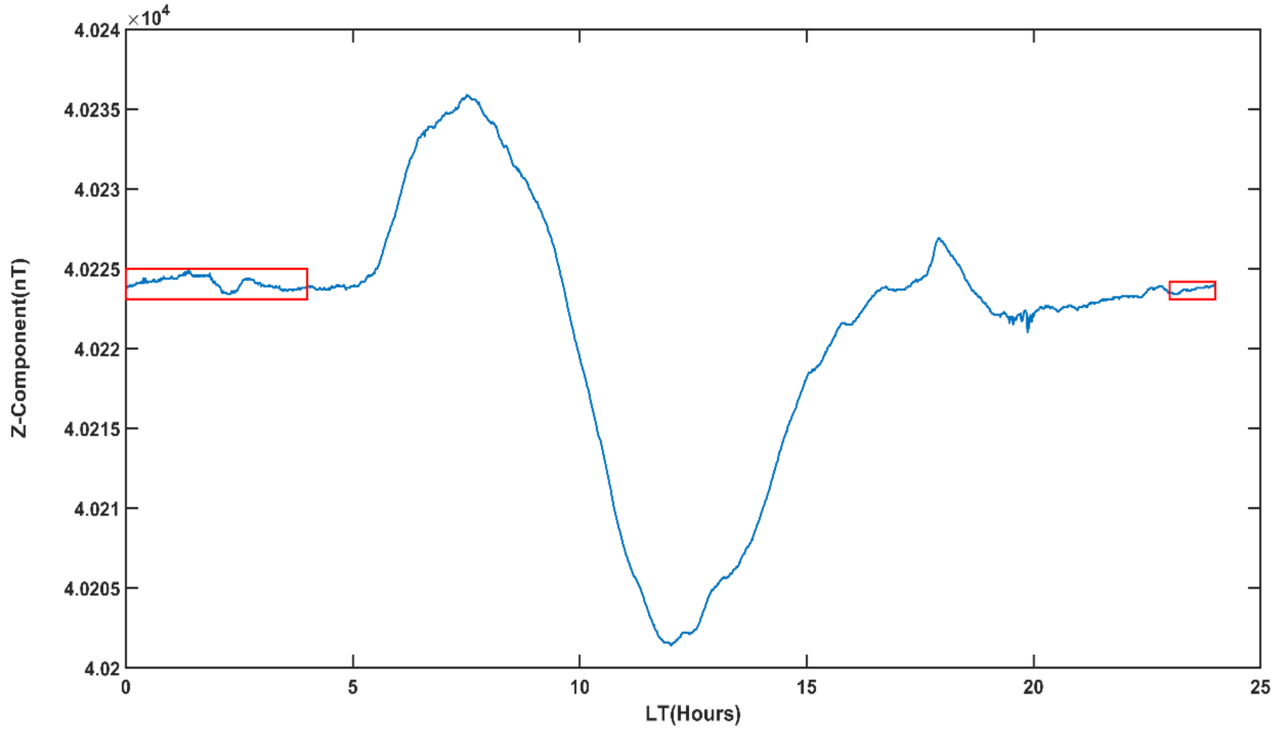

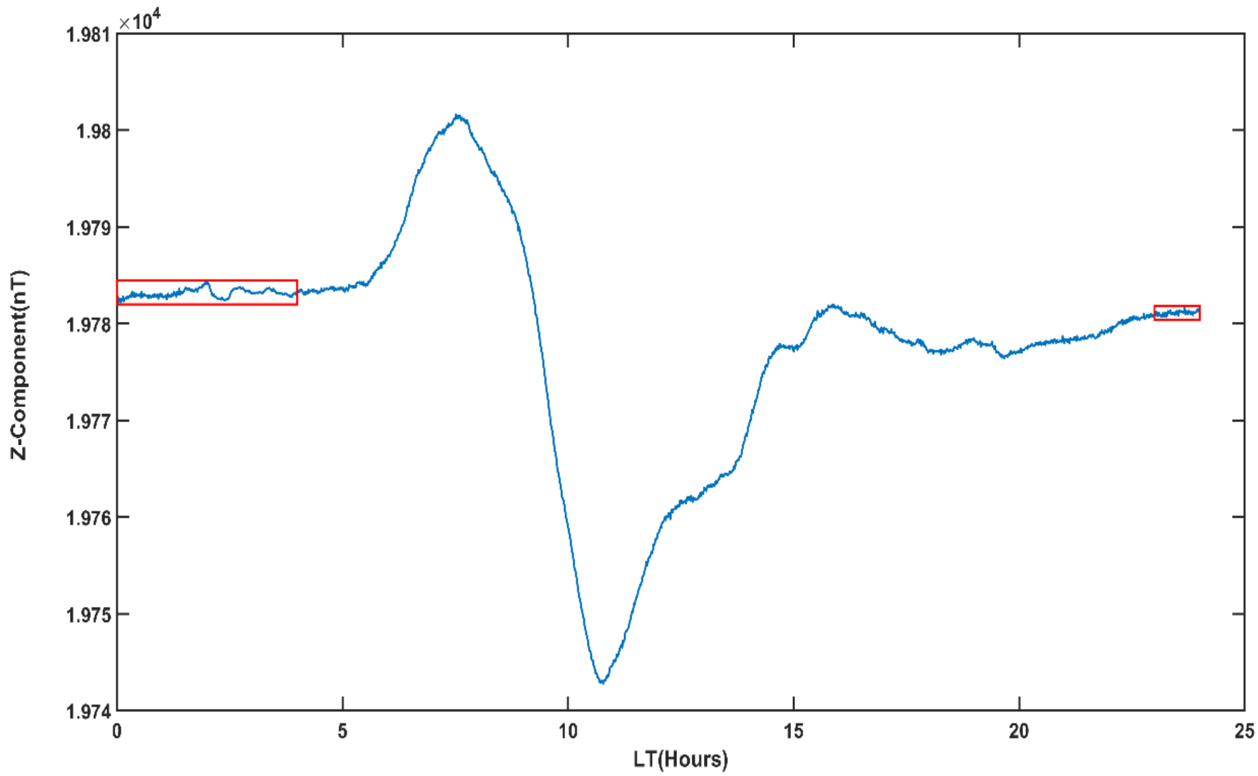

Figure 2a. The plot representing the one-day variation (24/08/2014) of geomagnetic field (z components) at Gulmarg (top) and Alibag (bottom) observatories during quiet conditions ($Kp=1^+$). The red rectangle box outlines the field values during 0 to 4Hrs and 23Hrs.

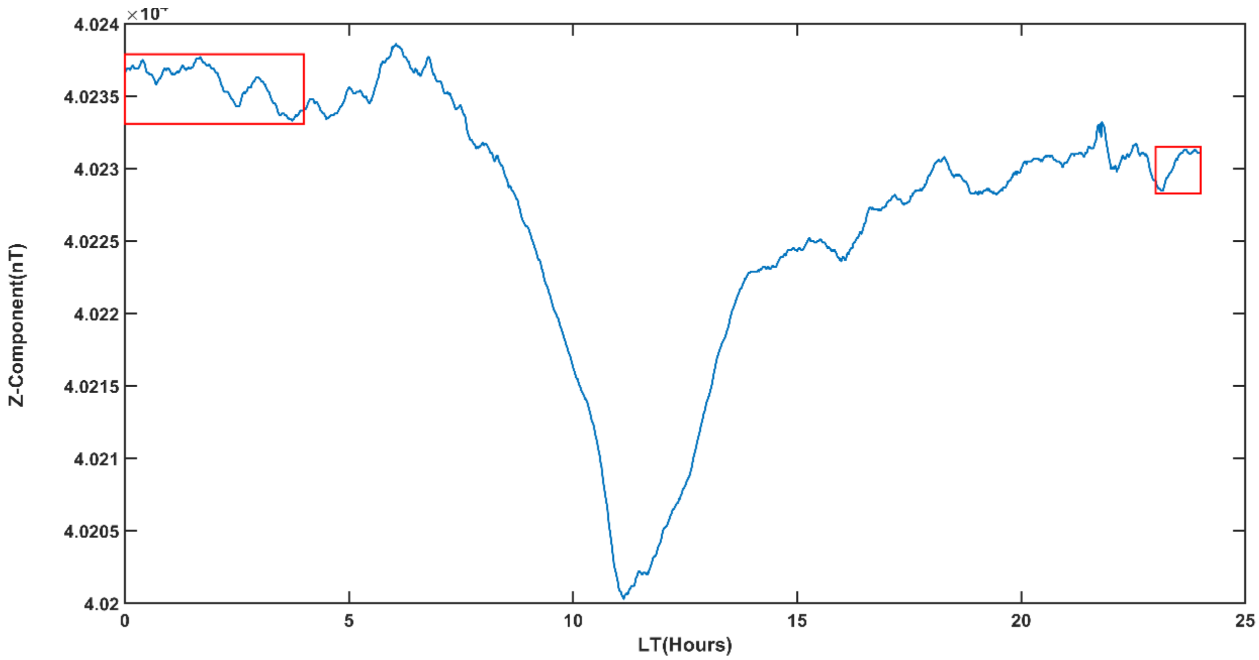

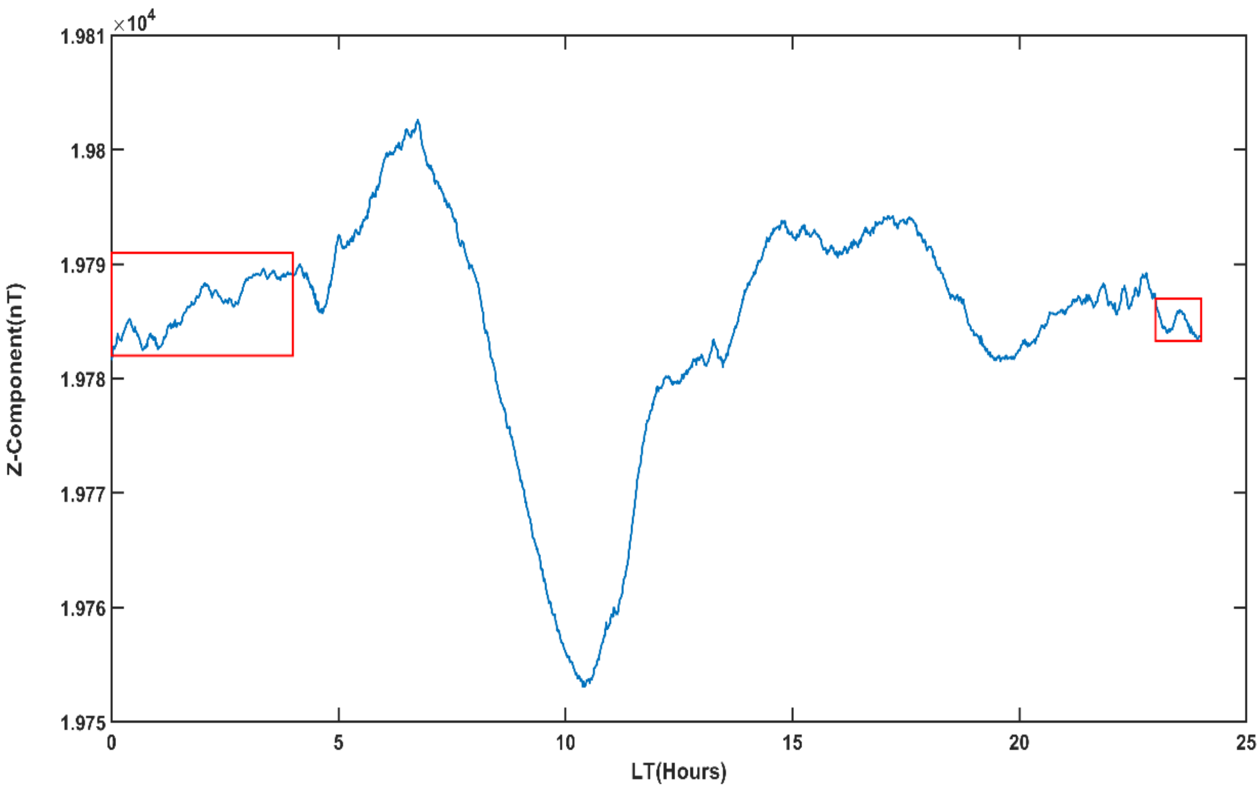

Figure 2b. The plot representing the one-day variation (28/08/2014) of geomagnetic field (z components) at Gulmarg (top) and Alibag (bottom) observatories during disturbed conditions ($Kp=3^+$). The red rectangle box outlines the field values during 0 to 4Hrs and 23Hrs.

The Dst index, a global index (Sugiura, 1964), quantifies the strength of the symmetric westward ring current encircling Earth during geomagnetic storms. It relies on H component data from four low-latitude ground observatories, located away from the influences of equatorial and auroral electrojets. Dst is computed by averaging the hourly deviations in the H component from its quiet time values at these observatories.

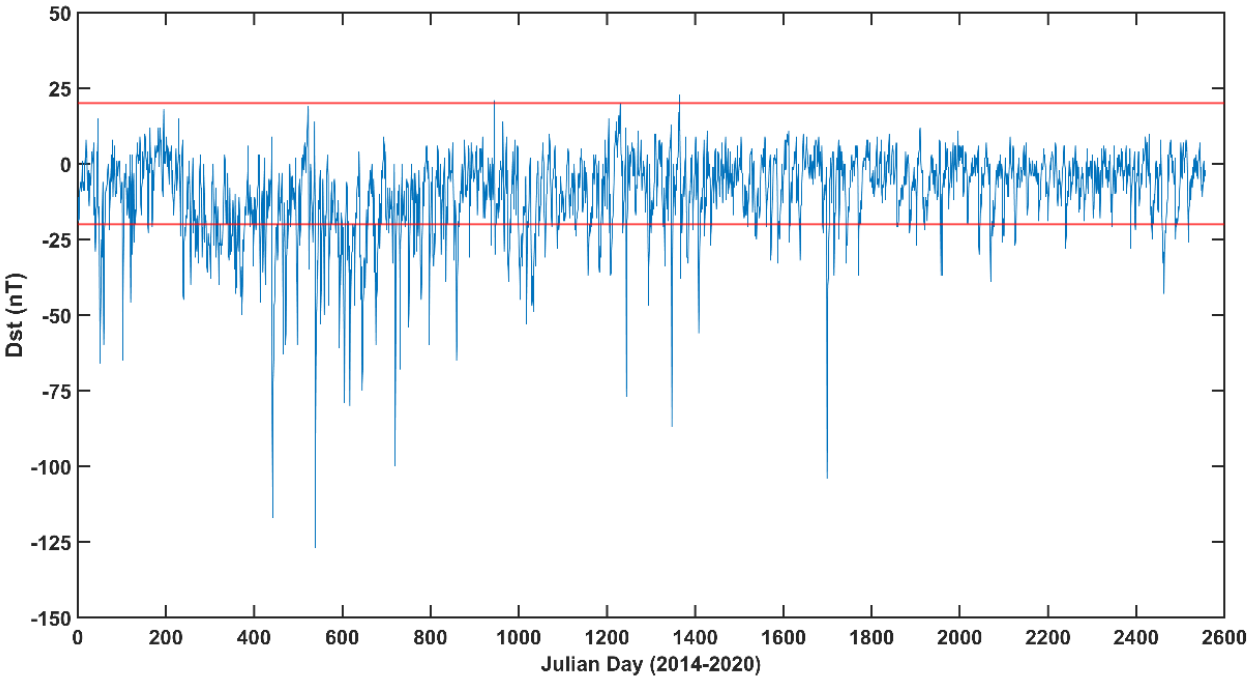

Figure 3. Variations in the disturbance storm time (Dst) index over the period from 2014 to 2020, exhibiting fluctuations between 50nT and -150nT.

To ensure that the data is minimally influenced by geomagnetic storm activities, the analysis focuses on Dst values within the range of -20nT to 20nT. This specific range, highlighted by a rectangular block in Figure 3, is selected for further processing to achieve more accurate and reliable results. Thus Kp and Dst indices serve as crucial parameters for dataset selection, with a preference for quiet conditions, where Kp < 2 and -20 < Dst < 20. This selection criterion ensures a robust volume of datasets covering the Indian region. During stormy periods, field amplitudes can exceed those of the lithosphere, posing challenges in isolating lithospheric field data. Consequently, a threshold of |Dst| < 20 is chosen to maintain data fidelity. Figure 3 illustrates the contrast in Dst values between storm and quiet conditions. Daytime introduces additional complexities due to active ionospheric currents, which can confound lithospheric models. To mitigate this interference, satellite passes during night time over the Indian region are favored for modeling. Specifically, the time-frame between 23:00 and 04:00 is selected to minimize ionospheric effects, as depicted in the accompanying Figure 4a, b. This strategic approach enhances the accuracy of geomagnetic field analysis by mitigating the influence of ionospheric currents during satellite measurements.

Test cases have been conducted to check ionospheric signatures across varying environmental conditions, encompassing both quiet and disturbed states during day and night periods. Magnetic data of 21 September 2014 (Figure 4a, top panel) and 9 November 2020 (Figure 4b, top panel), characterized by minimal geomagnetic activity (low Kp and Dst values), has been analyzed. Utilizing the CHAOS-7 geomagnetic field model (Finlay et al., 2020), the core, crust, and magnetosphere components were subtracted from the magnetic data acquired from a single pass of swarm satellite observations over Indian region. The residual signals are attributed to ionospheric origins, with their magnitude anticipated to be minimal for lithospheric modeling computations. Further similar test cases for the ionospheric field during disturbed conditions on May 8, 2014 (Figure 4a, bottom panel) and 22 November 2020 (Figure 4b, bottom panel), were undertaken, encompassing both daytime and nighttime intervals. The resultant signals have been plotted to illustrate the ionospheric field variations during quiet and disturbed periods, across day and night time as shown in Figure 4a, b. It can be seen from the figures, that during quiet conditions, amplitudes of the night time ionospheric signals are near zero while during the day time and disturbed time, there is considerable contribution from the ionospheric sources.

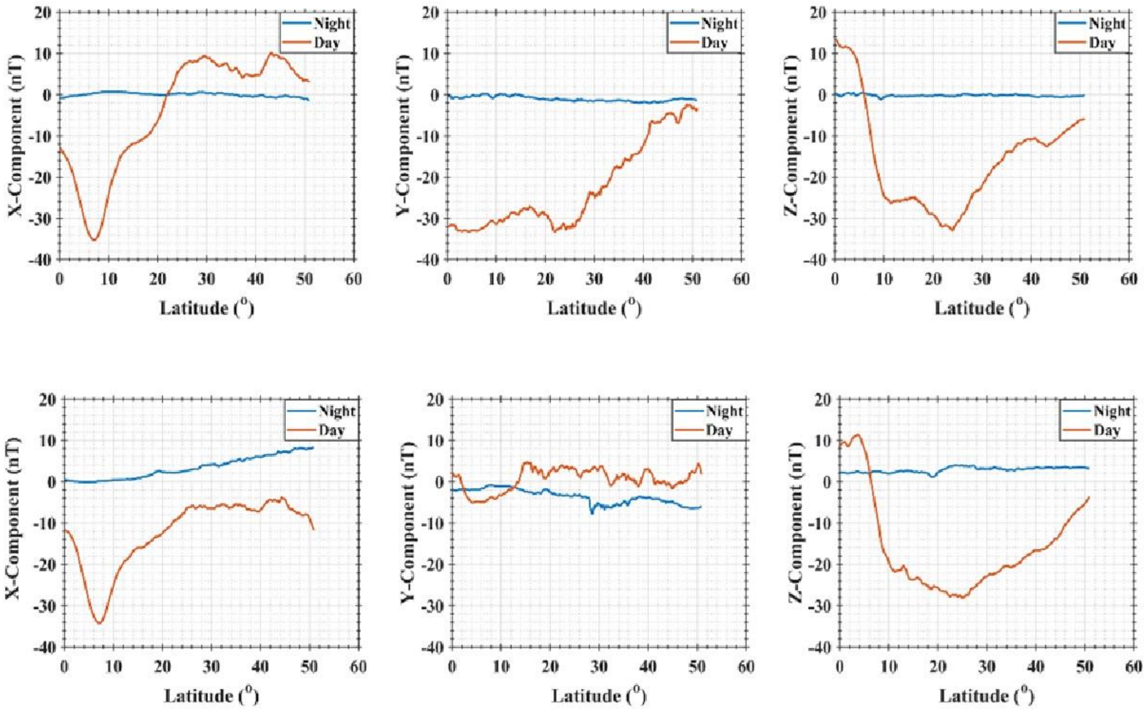

Figure 4a. The plot illustrating the vector component (X, Y, Z) of ionospheric field effects at day and night time during quiet (21/09/2014) (top panel) and disturbed conditions (08/05/2014) (bottom panel) .

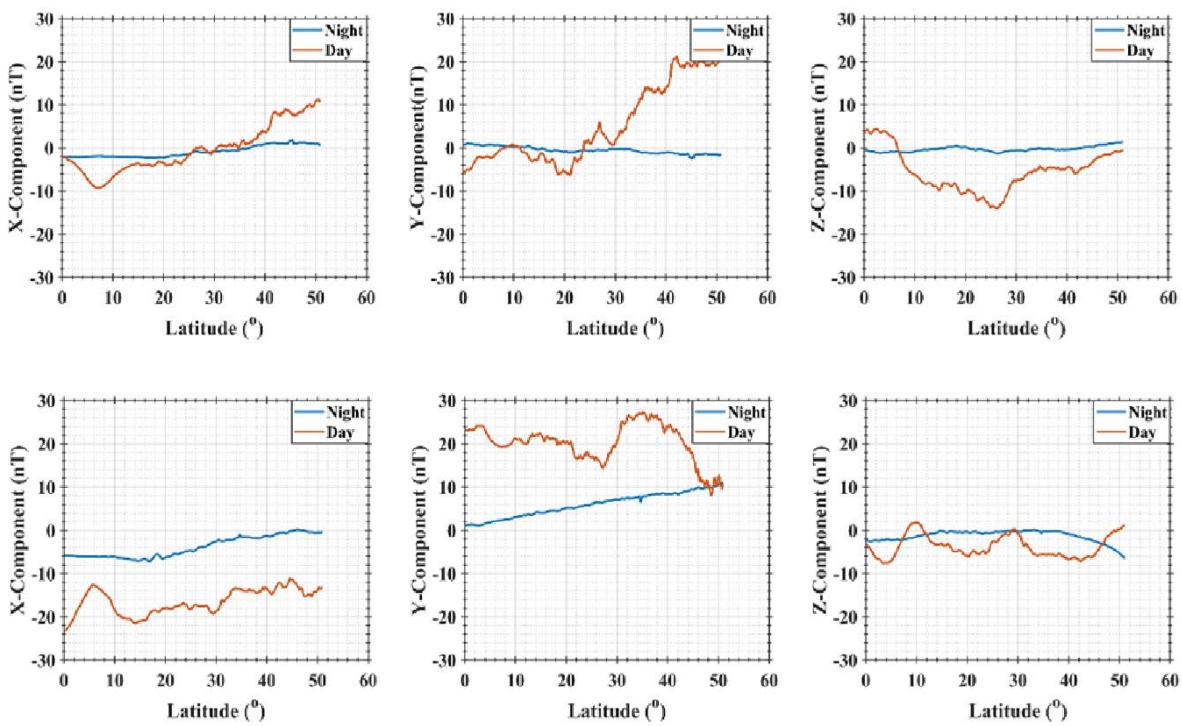

Figure 4b. The plot illustrating the vector component of ionospheric field effects at night and day time during quiet (09/11/2020) (top panel) and disturbed conditions (22/11/2020) (bottom panel) day.

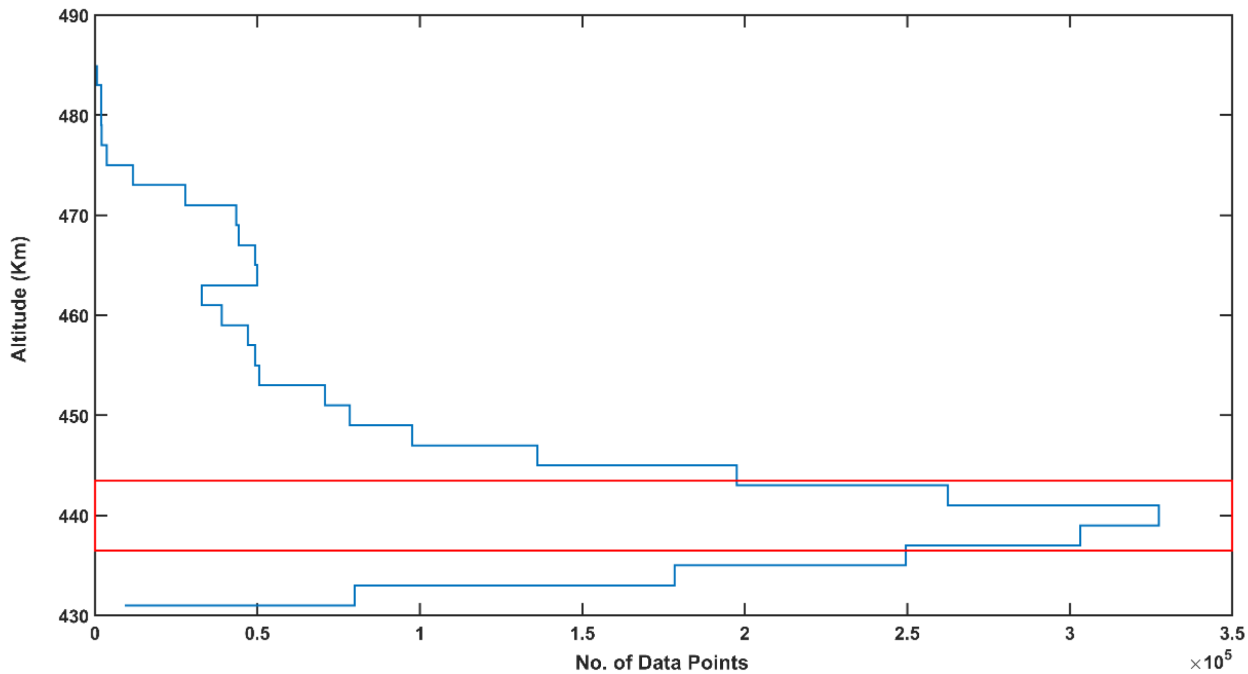

Figure 5. The observed data points by Swarm satellites (A and C) with respect to altitude during the quiet time conditions within the period 2014-2020, red rectangular box represent the selected data

Altitude selection

The Swarm satellite mission has been carrying out magnetic field measurements across multiple years, utilizing various orbital altitudes. Data availability during the span of 2014 to 2020 at different altitudes, after applying the environmental selection criteria as discussed above, is shown in Figure 5. A dataset consisting of over 22 lakh data points has been acquired from the Swarm A and C satellites, Level 1b data product. From this extensive dataset, a focused subset of over 8 lakh data points has been carefully selected. This selection process is based on low altitudinal data points within a precise altitude range of 437 km to 443 km, as highlighted with rectangular block in the Figure 5. This specific range of altitudes was chosen because it contains the largest concentration of observed data points and that the measurements taken at lower altitudes significantly enhance the amplitude of detected magnetic anomalies. In addition, data corresponding to the selected altitude falls in the time frame of low solar activity.

Background correction

The ionospheric effects can be minimized by selecting the international quiet days and taking the nighttime satellite passes as discussed above. To refine the model further, the contributions from non-essential fields - both the main field and residual external fields acting as the background field, need to be eliminated. This step is crucial in ensuring the accuracy of the regional model generated from satellite measurements. The core field, generated by electrical currents within the liquid outer core, exhibits magnitudes ranging in thousands of nanotesla. On the other hand, the external current system, stemming from ionospheric and magnetospheric dynamics and their interaction, typically varies from a few nanotesla to around a hundred nanotesla. A raw data plot of the z-component of the satellite data after applying the discussed selection criteria is shown in Figure 6, which represents a combination of fields arising from the core, external (residual), and lithosphere. To eliminate the background field arising from the core and the residual external (magnetosphere/ residual ionosphere), we employ the CHAOS-7 geomagnetic field model (Finlay et al., 2020), utilizing spherical harmonic expansions, which were subtracted from the observed data. The model expands the main field up to a 20-degree level, while restricting the external field to a 2-degree expansion. This approach effectively filters out unwanted field components, enabling a focused analysis of static lithospheric field.

The residual data (Figure 7) after applying the data selection criteria and removing the main magnetic field has a standard deviation of 3.4nT.

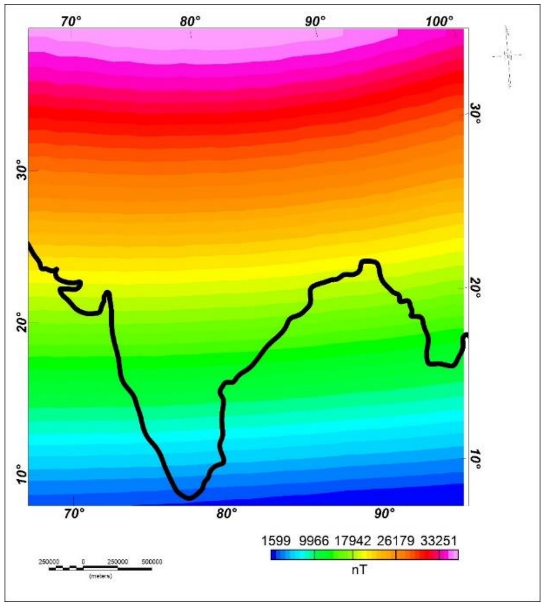

Figure 6. Raw data plot of vertical field (Bz) measured by Swarm satellites A and C, containing contribution from internal and external magnetic sources.

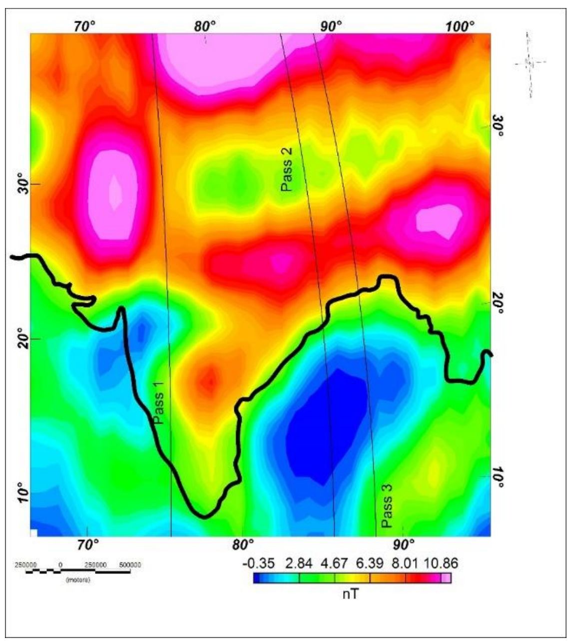

Figure 7. Raw data (Figure.6) from which the main field is removed using the CHAOS-7 geomagnetic field model. Lines, represent satellite passes which are discussed in Figure 8.

Temporal correction

Temporal selection involves the strategic selection of data which includes filtering data based on specific time intervals or periods of interest, ensuring accurate datasets for inversion. When examining adjacent satellite passes (during different time intervals) over the Indian region, inconsistencies were observed which may be attributed to the unmodeled contributions from magnetospheric currents, plasma pressure-driven electric currents (near the equator), gravity-driven current systems in the ionospheric F region, etc (Maus et al., 2007). The observed discrepancies result in unusual trends within the residual crustal field, exhibiting substantial fluctuations in magnitude. Given the satellite's orbit altitude of ~440 km, magnetometer readings are susceptible to influences from the external current system, potentially skewing the results. To counteract these effects, a meticulous approach involving visual inspection of individual satellite passes and comparison with adjacent passes to look for any first-order trend in the residual data was undertaken. Any such trends were removed from the data by fitting with a first order polynomial. This method aims to enhance the consistency between data from the adjacent passes. Apart from the trend removal, anomalous spikes or unidentified errors in field components are identified along individual passes, necessitating data smoothing techniques to rectify these irregularities. Spikes or high-frequency noises in the data along passes are removed by applying a low-pass filter. Trend and high-frequency noise removed data along three satellite passes (location in Figure 7) is shown in Figure 8. The final data after applying the above-discussed corrections had a standard deviation of 2.2 nT for computing the lithospheric magnetic anomalies through damped least square inversion.

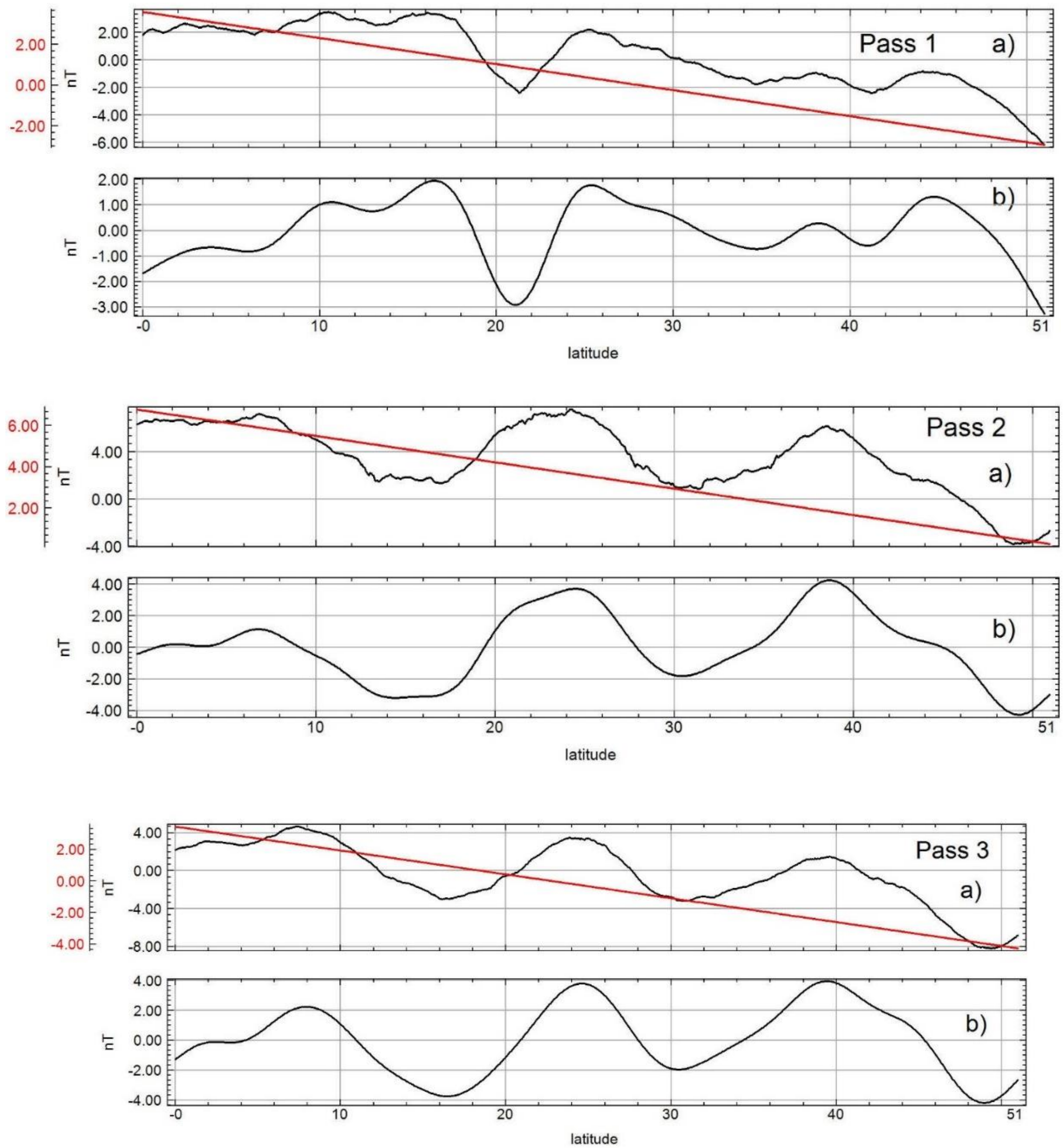

Figure 8. **(a)** Unprocessed data along satellite passes. Red line represents the fitted first order trend. **(b)** Processed data after removing the first-order trend and low pass filtering. Location of the passes shown in Figure 7

Apart from these corrections, the movement of electrically conductive ocean water due to tides creates what is known as the ocean tidal field. This tidal activity and ocean circulation (Manoj et al., 2006) generate magnetic signals that can reach amplitudes of up to 3 nanoteslas (nT) globally when measured at satellite altitudes (Tyler et al., 2003; Grayver and Olsen, 2019). However, over the Indian region, the effect of the tidal field is very minimal and is observed in the model provided by Yamazaki (2022) where the field is less than 0.4nT. Therefore correction for the tidal field is neglected. Extracting the weak lithospheric signal from satellite magnetic field observations is a complex task that requires advanced statistical methods and data processing techniques. One effective method uses spatial gradient information (East-West and North-South gradient), which is calculated by taking the differences between measurements at nearby locations. This approach helps to eliminate large-scale magnetic field contributions from non-lithospheric sources that are left over in the data, thereby highlighting the lithospheric signal (Olsen et., al 2017). By exclusively using this gradient data, it becomes possible to create accurate lithospheric field models without needing high-pass filtering or line leveling for each orbit.

DISCUSSIONS

The magnetic field measured by satellites is a superposition of magnetic field generated in the outer core, ionosphere and magnetospheric, magnetization of lithospheric rocks, induction fields generated by the currents flowing in the oceans and mantle. Previous studies of the spatial distribution of magnetic field suggests that at the orbital heights of satellites, only low frequency regional lithospheric anomalies with wavelengths equivalent to the orbital altitude and intensity of few tens of nT remains (Abramova and Abramova, 2014). Hence the isolation of lithospheric field from the strong background pose challenges when dealing the magnetic field measured onboard satellites. The reliability of detecting lithospheric field depends on the techniques selected for the removal of the other components. Hence the isolation of lithospheric field requires the knowledge of the background sources and noises. The specific task of identifying the lithospheric field that requires correction for external variations and main field, therefore often heavily rely on methods based on data selection and dedicated corrections. The generated global and local lithospheric models varies depending on the correction and reduction methodology adopted, the reason why several lithospheric models are generated. We have discussed some sources of errors and the basic corrections to remove the magnetic field contributions from these sources. We have categorized the selection and correction procedures under three groups of environmental selection which basically deals in minimizing the contribution from ionospheric sources, correction for main field and part of magnetospheric field under background removal and temporal selection including polynomial fitting, filter etc., to remove unmodelled external sources etc., in order to correct the measurement made by satellite data to develop regional lithospheric models. In the Lithospheric Magnetic Anomaly Map of India (LAMI-1) (Rawat et al., 2024), generated from 7 years of Swarm data, we have basically incorporated the environmental selection criteria and the back ground removal. The residual data after applying these two corrections were modelled through the damped least square inversion technique by expanding the Legendre polynomial of order $n = 6–50$. This model will be further improved by incorpor+ating the other corrections discussed in this article.

CONCLUSIONS

The Swarm satellite data collected over the period seven years from 2014 to 2020 has been rigorously analyzed to isolate the long-wavelength characteristics of the lithospheric magnetic field. This process involved comprehensive background and temporal corrections, along with meticulous environmental selection, to distinguish the lithospheric signals from various sources of noise and error. To ensure the accurate extraction of the lithospheric field, a series of practical tests and verifications were employed. Each technique described in this study has been carefully selected to enhance the identification and extraction of lithospheric features within the satellite data. The methods facilitated the effective filtering out of non-essential elements while preserving the lithospheric-scale signals.

Acknowledgements

The authors express sincere thanks to Prof A. P. Dimri, Director, IIG for his continuous encouragement and support and for the permission to publish this work. We thank the two reviewers and the Editor for their meticulous reviews and constructive criticisms, which have greatly improved the manuscript. Funds for carrying out this research at the Indian Institute of Geomagnetism is provided by the Department of Science and Technology (DST), Government of India, New Delhi.

Author contribution

The conception and design involved input from Monica Rawat and S. P. They also prepared the materials, collected the data, and analyzed it. Monica Rawat wrote the first draft of the manuscript, and correction and final editing of the manuscript was done by all the authors. All authors read and approved the final manuscript.

Data Availability

The data used in the current work is the low time resolution Swarm magnetic field data that is freely accessible to all users via ftp://swarm-diss.eo.esa.int. The Global magnetic field CHAOS model is freely accessible and available at https://www.space.dtu.dk/english/research/scientific_data_and_models/magnetic_field_models0. The Kp and Dst index data used in the current work for plotting is freely accessible to users via https://omniweb.gsfc.nasa.gov/

Compliance with ethical standards

The author declares that they have no conflict of interest and adhere to copy right norms.

References:

Abdellatif, A., Ghamry, E., Sobh, M. and Fathy, A., 2022. 2D lithospheric magnetic anomaly field over Egypt using gradient data of Swarm mission. Universe, 8(10), 530, https://doi.org/10.3390/universe8100530

Abramova, D.Yu. and Abramova, L.M., 2014. Lithospheric magnetic anomalies in the territory of Siberia (from measurements by the CHAMP satellite). Russ. Geol. Geophys., 55, 854-863, https://doi.org/10.1016/j.rgg.2014.06.005

Abramova, D.Yu., Filippov, S.V., Abramova, L.M. and Varentsov, Iv. M., 2014. Lithospheric magnetic anomalies in the Balkan region. Bulg. Geophys. J., 40, 50-64.

Agarwal, A.K., Singh, B.P., Rastogi, R.G. and Srinivasan, S., 1986. On utility of space-borne vector magnetic measurements in crustal studies. Phys. Earth Planet. Int., 41 260-268, https://doi.org/10.1016/0031-9201(86)90005-1

Fathy, A. and Ghamry, E., 2021. A two dimensional lithospheric magnetic anomaly field model of Egypt using the measurements from Swarm satellites. Geod. Geodyn., 12, 229-238, https://doi.org/10.1016/j.geog.2021.03.004

Finlay, C.C., Olsen, N., Kotsiaros, S., Gillet, N. and Tøffner-Clausen L., 2016. Recent geomagnetic secular variation from Swarm and ground observatories as estimated in the CHAOS-6 geomagnetic field model. Earth Planets Space**,** 68**,** https://doi.org/10.1186/s40623-016-0486-1

Finlay, C.C., Kloss, C., Olsen, N., Hammer, M.D., Tøffner-Clausen L., Grayver, A. and Kuvshinov, A., 2020. The CHAOS-7 geomagnetic field model and observed changes in the South Atlantic Anomaly. Earth Planets Space, 72, 156, https://doi.org/10.1186/s40623-020-01252-9

Grayver, A.V. and Olsen, N., 2019. The magnetic signatures of the M2, N2, and O1 oceanic tides observed in Swarm and CHAMP satellite manetic data. Geophys. Res. Lett., 46, 4230-4238. https://doi.org/10.1029/2019GL082400

Haines, G.V., 1985. Spherical cap harmonic analysis, J. Geophys. Res., 90, 2583-2591.

Hulot, G., Sabaka, T.J., Olsen, N. and Fournier, A., 2015. The Present and Future Geomagnetic Field. Treatise on Geophysics (Second Edition), 5(chapter 2) 33-7, https://doi.org/10.1016/B978-0-444-53802-4.00096-8

Langel, R.A., 1990. Global magnetic anomaly maps derived from POGO spacecraft data. Phys. Earth Planet. Int., 62, 208-30

Mandea, M. and Purucker, M. E., 2005. Observing, modeling, and interpreting magnetic fields of the solid earth. Surv. Geophys., 26 , doi:10.1007/s10712-005-3857-x

Manoj, C., Kuvshinov, A. and Maus, S., 2006. Ocean circulation generated magnetic signals. Earth Planet Space, 58, 429–437, https://doi.org/10.1186/BF03351939

Matzka, J., Stolle, C., Yamazaki, Y., Bronkalla, O. and Morschhauser, A., 2021. The geomagnetic Kp index and derived indices of geomagnetic activity. Space Weather, 19, e2020SW002641. https://doi.org/10.1029/2020SW002641.

Maus, S., 2010. Magnetic field model MF7. Available at: www.geomag.us/models/MF7.html

Maus, S., Luhr, H., Rother, M., Hemant, K., Balasis, G., Ritter, P. and Stolle, C., 2007.Fifth-generation lithospheric magnetic field model from CHAMP satellite meaurements. Geochem. Geophys. Geosyst., 8, Q05013, doi:10.1029/2006GC001521

Rawat, M., Anand, S.P., Fathy, A., Dimri,A.P. and Begum, S.K., 2024. Lithospheric Magnetic Anomaly map of Indian Sub-continent (LAMI-1) from Swarm satellite Data. J. Earth Syst. Sci., 133. https://doi.org/10.1007/s12040-024-02393-1

Olsen, N. and Stolle C., 2012. Satellite Geomagnetism. Annu. Rev. Earth Planet. Sci., 40, 441-465, 10.1146/annurev-earth-042711-105540

.Olsen, N., Hulot, G., Lesur, V., Finlay, C. C., Beggan, C., Chulliat, A. and Kotsiaros, S., 2015. The Swarm Initial Field Model for the 2014 geomagnetic field, Geophys.Res. Lett., 42, 1092–1098, doi:10.1002/2014GL062659

Olsen, N., Ravat, D., Finlay, C.C. and Kother, L.K., 2017. A high-resolution global model of the lithospheric magnetic field derived from CHAMP and Swarm satellite observations. Geophys. J. Int., 211, 1461-1477, https://doi.org/10.1093/gji/ggx381

Purucker, M.E. and Clark, D.A., 2011. Mapping and interpretation of the lithospheric magnetic field. In: Geomagnetic observations and models (pp. 311–337). Springer. https://doi.org/10.1007/978-90-481-9858-0_13

Purucker, M., Langlais, B., Olsen, N., Hulot, G. and Mandea, M., 2002. The southern edge of cratonic North America: Evidence from new satellite magnetometer observations. Geophys.Res. Lett., 29(15), 56, https://doi.org/10.1029/2001GL013645

Qiu, Y., Wang, Z., Jiang, W., Zhang, B., Li, F. and Guo, F., 2017. Combining CHAMP and Swarm Satellite Data to Invert the Lithospheric Magnetic Field in the Tibetan Plateau. Sensors, 17, 238, https://doi.org/10.3390/s17020238

Rawat, M., Anand, S.P., Fathy, A., Dimri, A. P. and Begum. S. K., 2024. Lithospheric Magnetic Anomaly map of Indian Sub-continent (LAMI-1) from Swarm satellite Data. J. Earth Syst. Sci., 133. https://doi.org/10.1007/s12040-024-02393-1

Sabaka, T.J., Toffner-Clausen, L. and Olsen, N., 2020. CM6: a comprehensive geomagnetic field model derived from both CHAMP and Swarm satellite observations. Earth Planets Space, 72, Article 80 . https://doi.org/10.1186/s40623-020-01210-5.

Shure, V., Parker, R.L. and Backus, G.E., 1982. Harmonic splines for geomagnetic modelling, Phys. Earth Planet. Int., 28 , 215-229, https://doi.org/10.1016/0031-9201(82) 90003-6.

Singh, B. P. and Rajaram, M., 1990. Magsat studies over the Indian region; Proc. Indian Acad.Sci. (Earth Planet Sci.), 99(4), 619-637, https://doi.org/10.1007/BF02840318

Stolle, C., Michaelis, I. and Rauberg, J., 2016. The role of high-resolution geomagnetic field models for investigating ionospheric currents at low Earth orbit satellites. Earth Planet Space., 68, 110, https://doi.org/10.1186/s40623-016-0494-1

Sugiura, M., 1964. Hourly values of equatorial Dst for the IGY. Ann. Int. Geophys. Year, 35, 9-45.

Thebault, E., Purucker, M., Whaler, K.A, Langlais, B. and Sabaka, T.J., 2010. The magnetic field of the Earth's lithosphere. Space Sci. Rev., 155, 95-127, doi: 10.1007/s11214-010- 9667-6

Thébault, E., Lesur, V., Kauristie, K. and Shore, R., 2017. Magnetic field data correction in space for modelling the lithospheric magnetic field. Space Sci, Rev., 206, 191-223, https://doi.org/10.1007/s11214-016-0309-5

Tyler, R., Maus, S. and Luhr, H., 2003. Satellite observations of magnetic fields due to ocean tidal Flow. Science, 299, 239-241.

Vervelidou, F., Thébault, E. and Korte, M., 2018. A high-resolution lithospheric magnetic field model over southern Africa based on a joint inversion of CHAMP, Swarm, WDMAM, and ground magnetic field data. Solid Earth, 9, 897–910, https://doi.org/10.5194/se-9-897-2018

Yamazaki, Y., 2022. Solar and Lunar daily geomagnetic variations and their equivalent current systems observed by Swarm. Earth, Planets Space, 74:99, https://doi.org/10.1186/s40623-022-01656-9

Zhang, J., Yang, X., Yan, J., and Wu, X., 2018. An analysis of the characteristics of crustal magnetic anomaly in China based on CHAMP satellite data. Geod. Geodyn**.,** 9, 328-333, https://doi.org/10.1016/j.geog.2018.04.004

Received on: 06-07-2024 ; Revised on: 21-10-2024; Accepted on: 21-10-2024